

# Thermophoretic motion behavior of submicron particles in boundary-layer-separation flow around a droplet

Ao Wang, Qiang Song,\* Bingqiang Ji, and Qiang Yao

Key Laboratory of Thermal Science and Power Engineering of Ministry of Education, Department of Thermal Engineering,  
Tsinghua University, Beijing 100084, China

(Received 26 August 2015; published 30 December 2015)

As a key mechanism of submicron particle capture in wet deposition and wet scrubbing processes, thermophoresis is influenced by the flow and temperature fields. Three-dimensional direct numerical simulations were conducted to quantify the characteristics of the flow and temperature fields around a droplet at three droplet Reynolds numbers ( $Re$ ) that correspond to three typical boundary-layer-separation flows (steady axisymmetric, steady plane-symmetric, and unsteady plane-symmetric flows). The thermophoretic motion of submicron particles was simulated in these cases. Numerical results show that the motion of submicron particles around the droplet and the deposition distribution exhibit different characteristics under three typical flow forms. The motion patterns of particles are dependent on their initial positions in the upstream and flow forms. The patterns of particle motion and deposition are diversified as  $Re$  increases. The particle motion pattern, initial position of captured particles, and capture efficiency change periodically, especially during periodic vortex shedding. The key effects of flow forms on particle motion are the shape and stability of the wake behind the droplet. The drag force of fluid and the thermophoretic force in the wake contribute jointly to the deposition of submicron particles after the boundary-layer separation around a droplet.

DOI: [10.1103/PhysRevE.92.063031](https://doi.org/10.1103/PhysRevE.92.063031)

PACS number(s): 47.55.-t

## I. INTRODUCTION

Particulate matter is a critical pollutant in atmospheric environments [1,2]. Wet scrubbing and wet deposition are efficient methods of removing particles from industrial flue gas and the atmosphere [3,4]. Particle capture by single droplet is the foundation of these two processes. Studies on single droplet capture are significant in developing industrial wet scrubbing technologies and in understanding the capacity and mechanisms of wet deposition in the atmospheric environment.

In the wet deposition and wet scrubbing processes, the fluid that carries particles flows around the droplet, during which particles can collide with the droplet surface during flow, under the inertia, interception, and Brownian mechanisms [5–7]. When the temperature between the environmental gas and the droplets is different, the motion of particles is affected by thermophoretic force. This force is the main mechanism through which submicron particles are captured by a droplet [8]. Bae *et al.* [9] evaluated the relative contribution of thermophoretic force in the process of wet deposition using the moment method and determined that the removal coefficient of  $1\ \mu\text{m}$  particles increased from  $10^{-7}$  to  $10^{-6}$  with a temperature difference of  $5\ ^\circ\text{C}$ . Pilat and Prem [10] calculated the single droplet capture efficiency of particles with different diameters when the difference in temperature was increased from  $5\ ^\circ\text{C}$  to  $60\ ^\circ\text{C}$ . The results showed that the capture efficiency of submicron particles increased by three orders of magnitude from 0.01 to 0.25.

Thermophoresis is a phenomenon in which aerosol particles suspended in a gas acquire a velocity in the direction of decreasing temperature due to collisions with the surrounding gas molecules [11–13]. The thermophoretic particle motion and deposition on walls in pipe flow or in flow between parallel

plates have been studied extensively [14–16], and research indicates that the movement of particles is mainly affected by two local parameters. One is the temperature gradient, which represents the intensity of thermophoresis, whereas the other is fluid velocity, which corresponds to the particle-carrying capacity of fluids. Particles tend to deposit on the wall, and deposition efficiency improves when the temperature gradient increases. When fluid velocity increases, the particles move farther to the downstream position and deposition efficiency decreases.

The flow field around the droplet varies from those of pipe flow and the flow between parallel planes. The main difference lies in the boundary-layer separation [17]. Nonetheless, the influence of boundary-layer-separation flow on the thermophoretic motion of submicron particles is disregarded in the calculation of thermophoresis capture efficiency [18]. For instance, the derivation process of the previous thermophoresis capture efficiency formula is based on the assumption that all the particles around the droplets are uniformly deposited on the droplet surface with the concentration of external flow. The values calculated by the previous formula display a relative deviation of 34%–76% in comparison with the experimental data [19], which is likely caused by the assumption regarding the uniform deposition of thermophoretic particles. In the actual process, movement and deposition on the droplet surface of submicron particles are not uniform under thermophoresis. Viswanathan [20] studied the thermophoretic motion of  $0.1\ \mu\text{m}$  particles in the flow around the droplet based on the assumption that flow field is axisymmetric. Under the effect of thermophoresis, the particles deposit on the droplets at the front and back, but the deposition ratio is not uniform. The proportion of particles deposited on the back of the droplets decreases from 48% ( $Re = 1$ ) to 20% ( $Re = 400$ ). Dau [21] simulated particle movement (Stokes number = 0.01) under the assumption of axisymmetric flow. When the flow around the droplet separates, the closed vortex ring structure at the

\*Corresponding author: [qsong@tsinghua.edu.cn](mailto:qsong@tsinghua.edu.cn)

rear of the droplet prevents particles from entering the wake if radiation force (such as thermophoretic and electrostatic forces) is not exerted. Particles cannot deposit after the flow separation point. The results presented by Viswanathan and Dau indicate that the changes in the flow and temperature field distributions caused by boundary-layer separation significantly influence particle movement and deposition. However, the two studies were conducted under axisymmetric flow. In the process of wet deposition and wet scrubbing, the droplet diameter is in the range of 0.5–2 mm and the Re is between 75 and 950 in free fall [22]. Several types of boundary-layer-separation flows are observed within this Re range [23–27]. When the Re is less than 210, the flow is axisymmetric and the wake is an axisymmetric vortex ring. When the Re is within the range of 210–270, the flow is a planar symmetry flow and the wake is a plane-symmetric vortex ring. When the Re is within the range of 270–500, the flow becomes unsteady flow and the wake sheds periodically. When the Re is more than 500, the position and intensity of vortex shedding are no longer fixed but random. The thermophoretic motion characteristics of submicron particles are unclear in the nonaxisymmetrical and unsteady flow field. In addition, such an investigation is important to understanding the thermophoretic capture mechanism of submicron particles by droplets and to establishing an accurate model to predict thermophoretic capture efficiency.

Three-dimensional direct numerical simulations are conducted in the current study to quantify the characteristics of the flow and temperature fields around a droplet at three droplet Reynolds numbers that correspond to three typical boundary-layer-separation flows (steady axisymmetric, steady plane-symmetric, and unsteady plane-symmetric flows). The thermophoretic motions of submicron particles are simulated in these cases. The motion patterns of particles, characteristics of deposition distribution on the droplet surface, and initial position of captured particles are analyzed as well. On this basis, the law and mechanism of the effect of boundary-layer-separation patterns on the thermophoretic motion of submicron particles are discussed.

## II. GOVERNING EQUATIONS AND NUMERICAL METHOD

### A. Equations of hydrodynamics and particle motion

In the wet deposition and wet scrubbing processes, the fluid that carries particles flows around the droplet, as shown in Fig. 1. When the temperatures of the droplet and the atmospheric gas differ, the particles deviate from the streamlines due to inertia, Brownian force, and thermophoretic

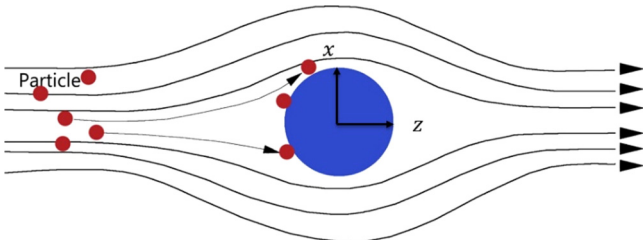


FIG. 1. (Color online) Schematic of particle capture by a droplet.

force; these particles collide with the droplet surface. The particles are assumed to be captured once they touch the droplet surface, which matches the common wet deposition and wet scrubbing processes. The droplet is assumed to be a sphere with a constant diameter because the reduction in diameter as a result of evaporation is negligible; actual deformation is slight in droplets with diameters smaller than 2 mm and circulation inside the droplet is weak compared with outside flow. Given the small velocity magnitudes compared with the local speed of sound, air is assumed to be incompressible. The coordinate system is established with the center of the droplet as the origin. The equations of hydrodynamics can be expressed as follows:

$$\vec{\nabla} \cdot \vec{u} = 0, \quad (1)$$

$$\frac{\partial \vec{u}}{\partial t} + (\vec{u} \cdot \vec{\nabla}) \vec{u} = -\frac{1}{\rho_f} \vec{\nabla} p + \nu \Delta \vec{u}, \quad (2)$$

$$\frac{\partial T}{\partial t} + (\vec{u} \cdot \vec{\nabla}) T = \frac{\lambda}{\rho_f c_p} \Delta T, \quad (3)$$

where  $t$  is the time,  $\vec{u}$  is the fluid velocity relative to droplet,  $\rho_f$  is the density of fluid,  $p$  is the pressure,  $\nu$  is the kinematic viscosity of fluid,  $T$  is the local fluid temperature,  $c_p$  is the specific heat capacity, and  $\lambda$  is the thermal conductivity.

The particles in the fluid flowing around the droplet are tracked with a Lagrangian formalism. As per the results of Pilat and Prem [10], the thermophoresis force is two to three magnitudes greater than the Brownian diffusion force for submicron particles when the temperature difference is above 10 °C. Therefore, Brownian diffusion force is ignored in this study. The particle motion equation is given as

$$m_p \frac{d\vec{v}}{dt} = \vec{F}_D + \vec{F}_T, \quad (4)$$

where  $m_p$  and  $\vec{v}$  are the mass and velocity of the particle center, respectively. The force  $\vec{F}_D$  is the drag force.  $\vec{F}_T$  is the thermophoretic force.

As the Re of submicron particles is far less than 1, the drag force of the particle can be well approximated to the classical Stokes drag.

$$\vec{F}_D = \frac{3\pi\mu_g d_p}{C_C} (\vec{u} - \vec{v}) + \frac{\mu_g \pi}{8} d_p^3 \nabla^2 \vec{u}, \quad (5)$$

where  $\mu_g$  is the fluid viscosity,  $d_p$  is the particle diameter, and  $C_C$  is the Cunningham correction factor. In this equation, the first term is the Stokes drag; the second term is the force related to pressure gradient and is proportional to the cube of the particle diameter. As the particle diameter decreases, the second term decreases sharply relative to the Stokes drag. In the simulation of this paper, for a particle with diameter of 0.1  $\mu\text{m}$ , the magnitude of the Stokes drag is about  $10^4$  times larger than the second term. Thus, the second term is neglected in Eq. (5).

$$C_C = 1 + \frac{2\lambda}{d_p} \left[ 1.257 + 0.4 \exp\left(-\frac{0.55d_p}{\lambda}\right) \right], \quad (6)$$

where  $\lambda$  is the mean free path of the gas.

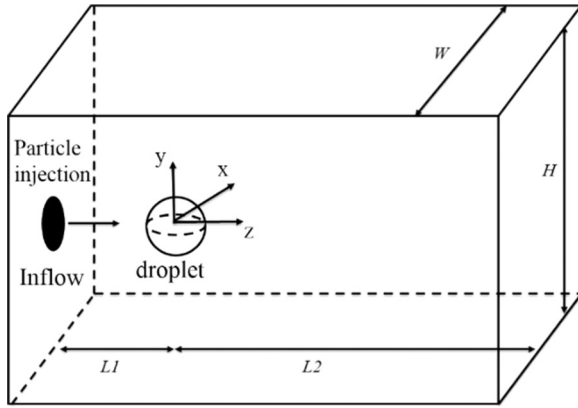


FIG. 2. Schematic of the computation domain.

The thermophoretic force can be expressed as follows:

$$\vec{F}_T = -D_{T,p} \frac{1}{T} \nabla T, \quad (7)$$

where  $D_{T,p}$  is the thermophoretic coefficient. The thermophoretic coefficient used in the simulation is suggested by Talbot [28]:

$$D_{T,p} = \frac{6\pi d_p \mu_g^2 C_s (K + 2C_t \lambda / d_p)}{\rho_f (1 + 6C_m \lambda / d_p) (1 + 2K + 4C_t \lambda / d_p)}, \quad (8)$$

where  $C_s = 1.17$ ,  $C_t = 2.18$ ,  $C_m = 1.14$ ,  $K = k_f / k_p$ ,  $k_f$  is the gas thermal conductivity, and  $k_p$  is the particle thermal conductivity.

### B. Numerical methods and meshing parameters

In this study, the air-carrying particles move around the droplet. The air temperature is assumed to be constant at 110°C. The droplet temperature is assumed to be constant at 10°C. The droplet diameter is fixed at 2 mm. The particle diameter is 0.1 μm. The flow and temperature fields are simulated at three representative Re values (150, 250, and 300) that correspond to three typical boundary-layer-separation flows. Re is changed by altering the inlet flow velocity.

A commercial finite volume solver (ANSYS FLUENT V14.5) is employed to solve the three-dimensional Navier-Stokes equation [Eqs. (1)–(3)] of air and the particle motion equation [Eq. (4)] directly. The computational domain is shown in Fig. 2. The spherical droplet is placed closer to the inlet than to the outlet in the domain, and the wall is set as the boundary condition of the droplet. The air flows into the domain along the  $z$  axis from the left plane ( $x, y$ ). The inlet is set as the inlet boundary condition, and the pressure outlet is a free boundary condition for an unconfined flow, such as in the present simulation. The other surfaces in the domain are set as the wall boundary condition. The pressure-based solver is applied. The SIMPLE algorithm, which combines pressure and velocity corrections to enforce mass conservation, is then employed. For the spatial discretization of pressure and momentum, the second-order scheme and QUICK scheme are applied, respectively. When  $Re < 270$ , the flow is in the steady regime and the time derivatives in Eqs. (2) and (3) are neglected. When  $Re > 270$ , the unsteady equations are solved using a second-order implicit time integration scheme.

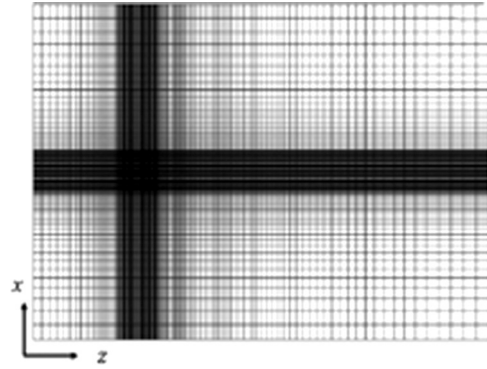


FIG. 3. Middle plane of the computational grids. The flow direction is parallel to the  $z$  axis and perpendicular to the  $x$  and  $y$  axes, respectively.

Particles are injected uniformly or individually into the domain from the projection of droplets onto the inlet surface. The number of particles injected once is 32 580. The discrete particle model is employed to trace the movement and position of particles. If the flow is in the unsteady regime, then the simulation of particle movement and the update of flow field occur simultaneously. After all particles are traced, the particle motion trajectories and deposition location can be obtained and analyzed statistically. The capture efficiency of particles can be determined by recording the total number of captured and released particles.

Structured meshes are employed to simulate the flow around the droplet instead of easy-to-use unstructured meshes, because mesh quality significantly influences the accuracy of the calculation results. The domain has to be decomposed into several subdomains, through which structured grids can be generated around the sphere (Fig. 3). The grids are structured and consist of body-fitted hexahedral control volume elements.

The block effect of computational domain size and the resolution of grids influence the accuracy of flow simulation [29]. The drag coefficient ( $C_D$ ) is a dimensionless quantity to quantify the drag of an object in a fluid environment. The Nusselt number (Nu) is the ratio of convective to conductive heat transfer within a fluid.  $Nu = hD/k_f$ , where  $h$  is the convective heat transfer coefficient,  $D$  is the droplet diameter. The drag coefficient and the Nusselt number of the flow around a droplet are usually regarded as evaluation parameters to test the accuracy of flow and temperature field simulation. Therefore, the drag coefficient and Nu are calculated under different domain sizes and grid resolutions. We select the most suitable domain size and grid resolution for our simulation by comparing the drag coefficients and the Nu acquired in previous experiments under the same condition. With the selected grids and the corresponding numerical method, the obtained drag coefficient and the Nu correspond to the experimental results perfectly. The relative deviation of the calculation is within 5% in the steady flow regime with low Re and in the unsteady flow regime with high Re. Hence, the flow and temperature fields around the droplet obtained via simulation are consistent with the actual flow and temperature fields (Fig. 4).

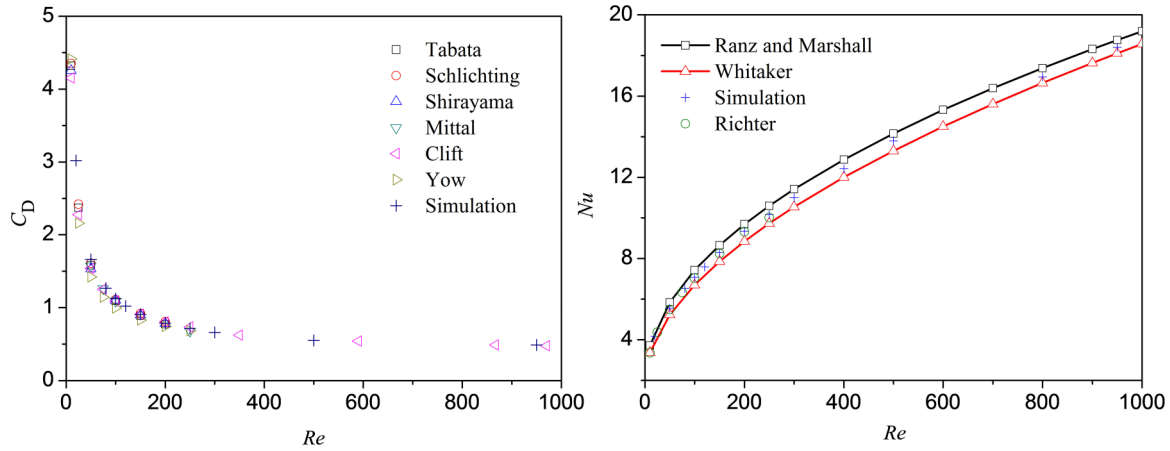


FIG. 4. (Color online) Comparison of the drag coefficient and Nusselt number obtained from experiments [29] with the results of the present study for the flow around a sphere at different Reynolds numbers.

**III. CHARACTERISTICS OF FLOW AND TEMPERATURE FIELDS**

The experiments and simulations of flow around a sphere indicate that the boundary layer begins to separate when  $Re > 20$ . Moreover, flow patterns vary when  $Re$  increases within the range of 20–1000 [23–27]. When  $20 < Re < 210$ , the flow is steady and axisymmetric and the wake is a closed axisymmetric vortex ring. When  $210 < Re < 270$ , the flow remains steady but is planar symmetric. The flow field is divided into two similar parts by the symmetry plane. When  $Re > 270$ , the flow becomes unsteady. Vortex shedding is initiated behind the droplet. In this study, we conduct our simulation with three representative  $Re$  values (150, 250, and 300). The simulation results show that the flow is steady and axisymmetric when  $Re = 150$ . When  $Re = 250$ , the flow is steady and planar symmetric. When  $Re = 300$ , hairpin vortices are shed from a fixed position at the rear of the droplet and the flow is planar symmetric. The simulated flow patterns correspond to the experimental observations in all  $Re$  ranges.

In addition, the simulated drag force coefficients,  $Nu$ , and the corresponding  $Re$  coincide with the experimental results as presented in Sec. II B, thus confirming that the simulated flow and temperature fields are identical to the actual ones.

Figure 5 shows the streamlines, temperature field, and temperature gradient field at  $Re = 150$ . The temperature field and temperature gradient field were generated by the contour display function of the software. The flow and temperature distribution are axisymmetric, and the wake is a closed axisymmetric vortex ring. A thin temperature boundary layer exists at the front of the droplet. The temperature gradient distribution shows that this gradient is maximized around the front droplet surface. The temperature gradient around the rear droplet surface is approximately one third of that around the front surface; nonetheless, it remains considerably larger than the temperature gradient in the vortex and in the outer field.

When  $Re = 250$ , the flow is steady planar symmetric. Figures 6(a) and 6(b) show the streamlines constructed from the in-plane velocity vectors in planes  $(y, z)$  and  $(x, z)$ , respectively.

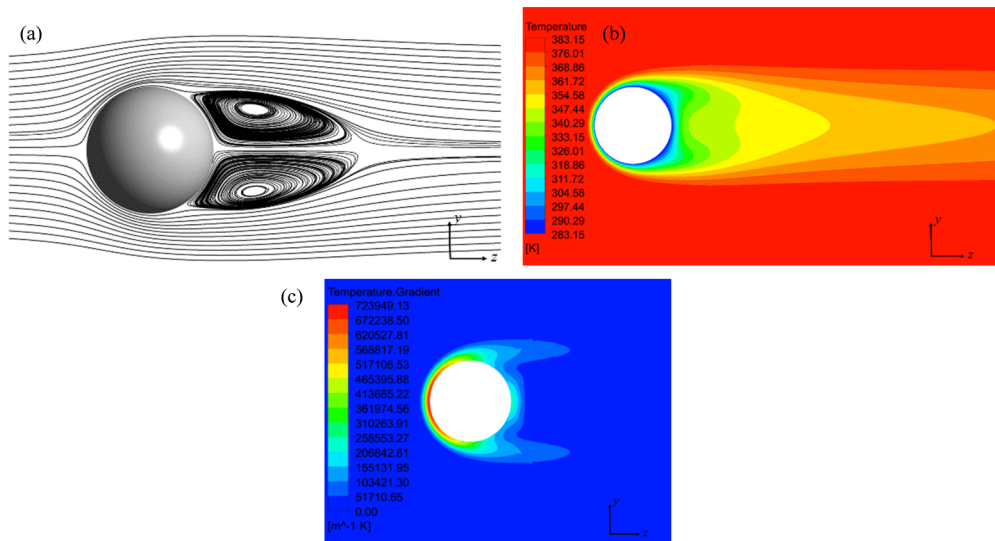


FIG. 5. (Color online) Streamlines and temperature distribution around the droplet at  $Re = 150$ . (a) Axisymmetric streamlines; (b) temperature field; (c) temperature gradient field.

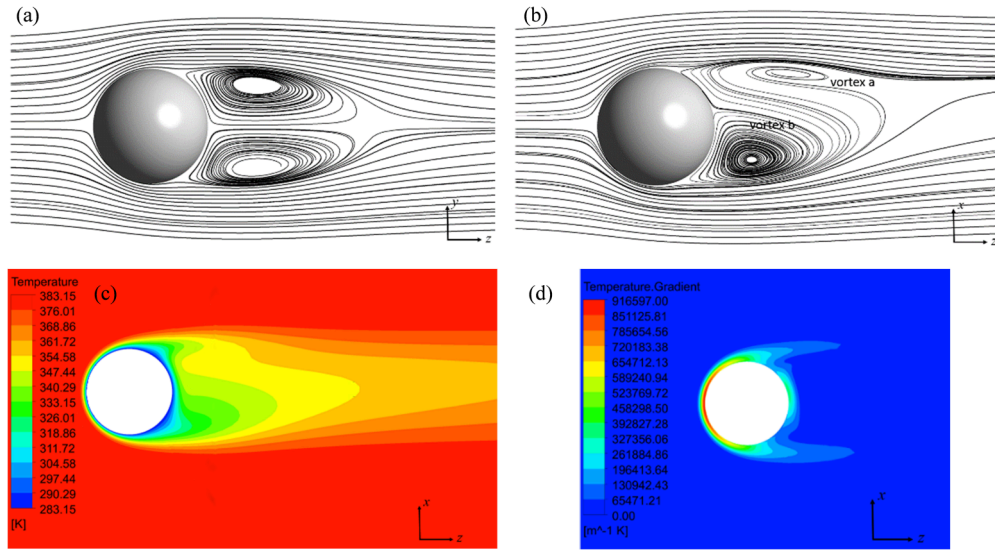


FIG. 6. (Color online) Streamlines and temperature distribution around the droplet at  $Re = 250$ . (a) Streamlines at the plane  $(y,z)$ ; (b) streamlines at the plane  $(x,z)$ ; (c) temperature field at the plane  $(x,z)$ ; (d) temperature gradient field at the plane  $(x,z)$ .

Figure 6(a) indicates that the flow field is symmetric at plane  $(x,z)$ , which divides the flow field across the center. There are out-of-plane velocity components in Fig. 6(a) so that the lines constructed in this manner do not correspond to true three-dimensional streamlines. However, since Fig. 6(b) corresponds to the  $(x,z)$  symmetry plane, there are no out-of-plane components, in this case, representing true streamlines. Considering Fig. 6(b), it is apparent that the toroidal vortex

has tilted. It is also clear from the difference between the top and bottom of the vortex ring that its size is not constant in the azimuthal direction. Additionally, the toroid is no longer a closed separation bubble; the upper spiral is actually fed by the fluid originating from upstream while the lower spiral releases the fluid into the wake after sending the fluid up and around the upper spiral. Although the top and bottom of the vortex ring belong to the same vortex and are interlinked [25], we label

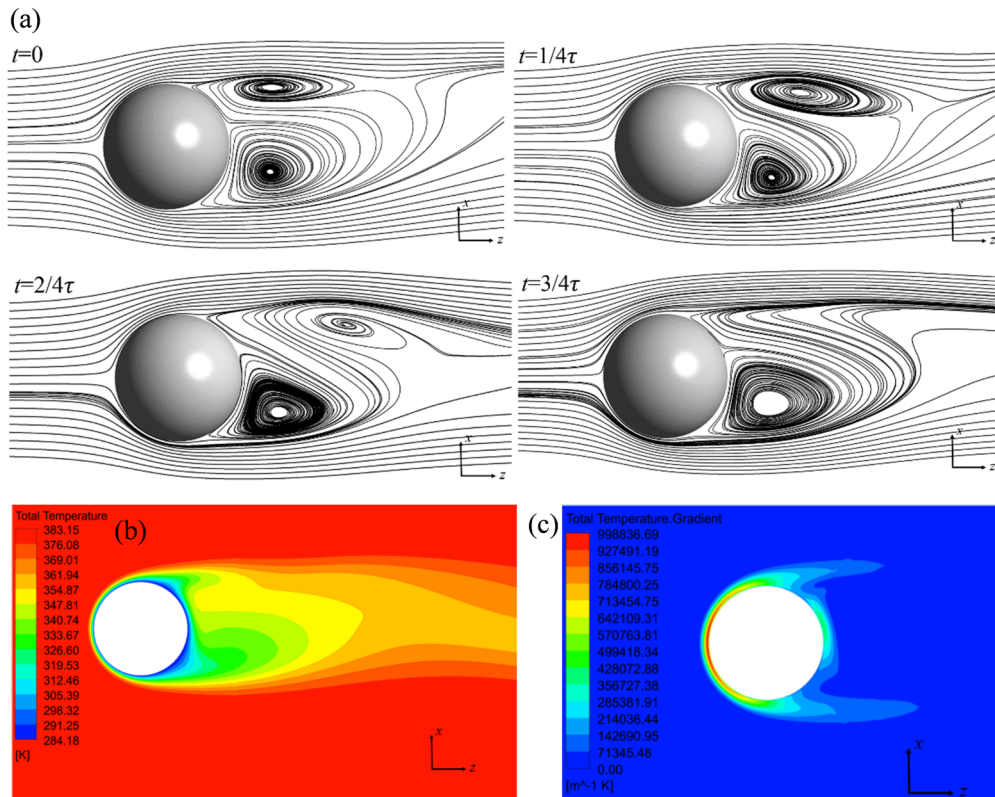


FIG. 7. (Color online) Streamlines and temperature distribution around the droplet at  $Re = 300$ . (a) Streamlines at the plane  $(x,z)$  for every quarter period; (b) temperature field at the plane  $(x,z)$  when  $t = 1/4\tau$ ; (c) temperature gradient field at the plane  $(x,z)$  when  $t = 1/4\tau$ .

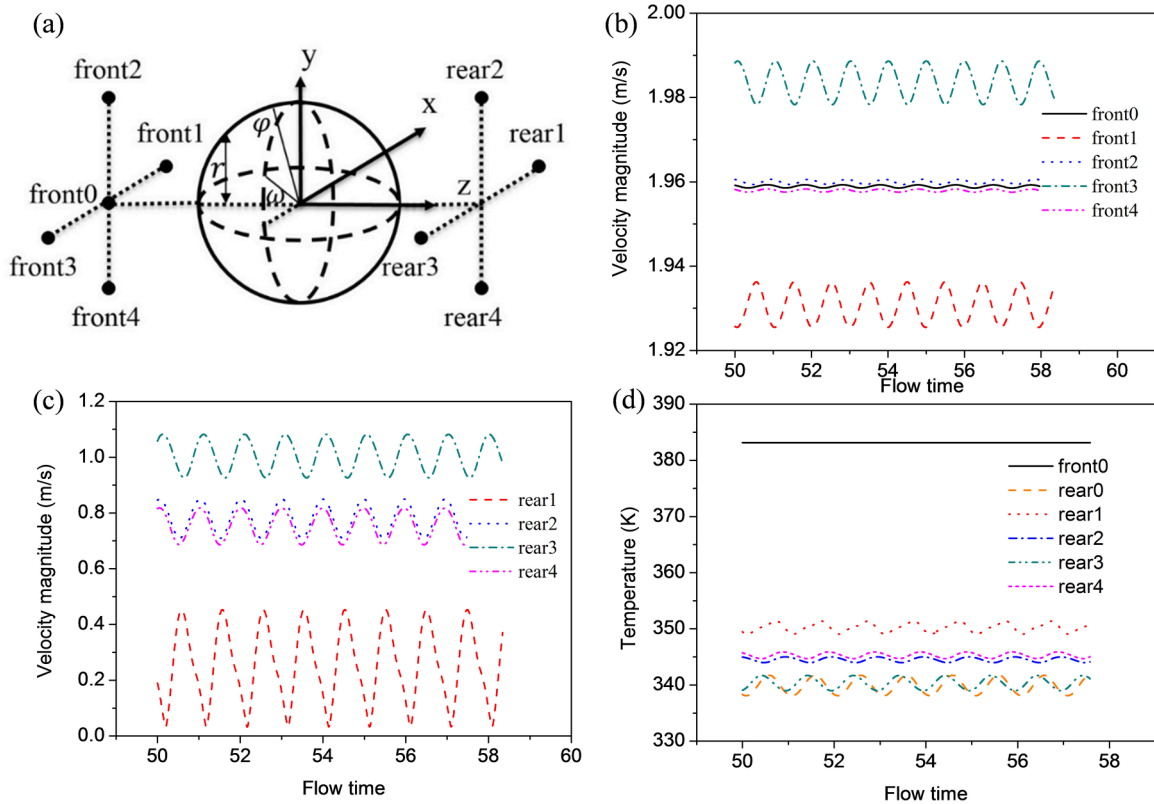


FIG. 8. (Color online) Velocity magnitude and temperature at monitoring points. (a) Distribution of monitoring points at the front and rear of the droplet; (b) velocity magnitude at front monitor points; (c) velocity magnitude at rear monitor points; (d) temperature at monitor points.

the top and bottom parts of the vortex shown in plane  $(x, z)$  as vortices  $a$  and  $b$  for convenient description.

The flow is planar symmetric at  $Re = 250$ , as is the temperature field distribution around the droplet. Figures 6(c) and 6(d) show the distribution of temperature and of the temperature gradient in symmetry plane  $(x, z)$ , respectively. Vortex  $b$  has a stronger convection capability; thus, its temperature distributes evenly. The temperature gradient [Fig. 6(d)] is displayed. The largest temperature gradient region at the droplet rear moves in the direction of vortex  $a$ . The largest temperature gradient region is still found only in the vicinity of the droplet surface. The temperature gradient is very small in the vortex and outer flow, as with that in the axisymmetric flow at  $Re = 150$ . Nonetheless, the temperature boundary layer thins and the temperature gradient increases at  $Re = 250$ .

When  $Re = 300$ , the flow behind the droplet enters the unsteady planar symmetric state caused by vortex shedding. In this paper, the symmetric plane is adjusted to plane  $(x, z)$  for convenient observation and description. Figure 7(a) shows the streamlines in the symmetric plane  $(x, z)$  at four moments in the growing to shedding process of a wake in a flow period. The growing ( $t = 0$  and  $t = 1/4\tau$ ) to shedding ( $t = 2/4$  and  $3/4\tau$ ) process of a vortex is observed in this figure, where  $\tau$  is the period of vortex shedding. Although the flow transforms into the unsteady state, the distributions of streamlines [Fig. 7(a)], temperature [Fig. 7(b)], and temperature gradient [Fig. 7(c)] all resemble those at  $Re = 250$  topologically. However, the specific values vary periodically over time.

In previous studies [26] on flow around a sphere, monitoring points were positioned in the wake of the sphere to record the

velocity magnitude for quantifying the flow rules in the wake. However, the variation of the velocity in front of the sphere was not considered. Some particles can be captured at the front part of a droplet. Therefore, monitoring points are placed in front of the droplet in addition to the rear monitoring points in the present study to investigate the variation of velocity and temperature with time. The arrangement of monitoring points is shown in Fig. 8. Five points are located on the axis parallel to the  $x$  and  $y$  axes in front of the droplet. The spacing between points denotes the droplet radius. The plane on which front0 to front4 are located is one droplet diameter from the droplet center. Four monitoring points are positioned behind the droplet. The distributions of rear1 to rear4 and front1 to front4 are symmetrical relative to plane  $(x, y)$ . The velocity magnitudes of the monitoring points at the front and at the rear of the droplet oscillate periodically because of vortex shedding, as indicated in Figs. 8(b) and 8(c). The flow time is dimensionless as the real flow time is divided by the time of the vortex shedding period. The difference in the mean velocities of front0 to front4 is slight at only 0.053 m/s. The amplitude of velocity oscillation at each front point is less than 0.01 m/s. By contrast, the amplitude at the rear points is greater than 0.2 m/s. The oscillation amplitudes at the front points are significantly smaller than those of the rear points. The temperature oscillations at the front and rear points are exhibited in Fig. 8(d). The temperature at the front points is represented by that at front0 because the temperature at front0 to front5 does not change with time. Although the temperature at the rear of the droplet oscillates periodically, the maximum relative change with time is only 5%. Overall, the effect of

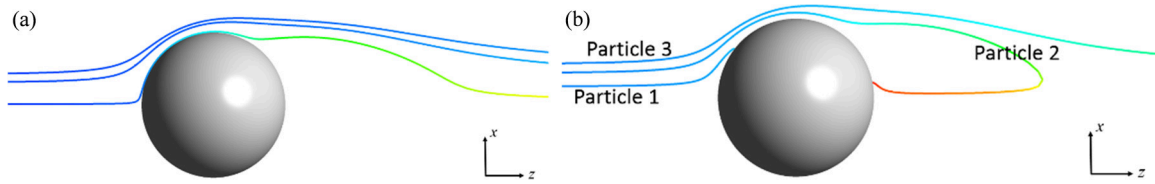


FIG. 9. (Color online) Trajectories of particles at  $Re = 150$ . (a) Trajectories of particles immune to thermophoresis; (b) trajectories of particles subjected to thermophoresis.

vortex shedding at the rear of the droplet on the front flow and temperature field is weak. Therefore, the motion and deposition of particles at the droplet front can be considered immune to wake influence.

#### IV. BEHAVIOR OF PARTICLE MOTION AND DEPOSITION IN STEADY AXISYMMETRIC FLOW

To understand the thermophoretic motion behavior of particles in boundary separation flow, the trajectories of particles that are immune to and are subjected to thermophoresis were studied to reveal the thermophoretic effect on particle motion and deposition. In addition, the particle motion pattern, deposition distribution on droplet surface, and distribution of the initial position of captured particles were explored under the actual condition of flow and temperature distribution.

At  $Re = 150$ , particle motion is two-dimensional planar because the flow is axisymmetric. Figure 9 illustrates the trajectories of the particles at  $Re = 150$ . The colors of the trajectories change from blue to red, thus representing the residence time of particle motion qualitatively. Particle diameter in this study is only  $0.1 \mu\text{m}$ ; therefore, the corresponding Stokes number is less than the critical Stokes number, at which the particle is captured because of its own inertia. Without thermophoresis, the particle cannot be captured at the droplet front whenever it is injected, as shown in Fig. 9(a). Meanwhile, the vortex ring is closed behind the droplet, and the particle cannot enter the wake but flows downstream.

The motion pattern of particles can be divided into three categories with thermophoresis, as per Fig. 9(b). The particle injected from the vicinity of the central axis line (Particle 1) is captured by the droplet surface before the flow separation point. The particle injected from the position that is at a certain distance from the central axis (Particle 2) enters the closed vortex ring, flows in the vortex region, and is eventually captured on the back of the droplet. If the particle is injected further from the central axis (Particle 3), it bypasses the droplet and cannot be captured. In the previously described cases of particle motion, the particles that are injected closer to the center axis of the droplet are captured easily. Figure 10 shows the distribution of the initial positions of captured particles. The black circle boundary is the projection of the droplet on the inlet plane and also represents the area in which all particles are injected. The black dots represent the initial positions of the particles captured before the flow separation point, whereas the blue dots represent the initial positions of the particles captured after the flow separation point. The initial positions of particles form a continuous region called the main capture region. The particles injected beyond this region cannot be captured at  $Re = 150$ . The initial region of captured particles is circular

because of the axisymmetric distribution of flow and temperature. The deposition distribution of particles on the droplet surface is circular as well. The results for particle motion and deposition behaviors are consistent with those calculated by the model, which assumes an axisymmetric flow [20].

Figure 11 shows that the thermophoresis forces exerted on the particles moving in three motion patterns change over time. The thermophoresis force vector is inclined toward the droplet center from the position of the particle. The thermophoresis force exerted on Particle 1 is the strongest among the three particle motion patterns. Moreover, the thermophoretic force exerted on the particle increases as the particle gradually approaches the droplet surface. The thermophoretic force reduces later on because the particle moves downstream of the droplet at which the temperature gradient is less than that in the vicinity of the front stagnation point. The particle is subject to a strong thermophoretic force in the flow process in the vicinity of the droplet; thus, this particle is deposited directly on the front of the droplet. Particle 2 is also subject to a strong thermophoretic force when moving to the vicinity of the droplet; this force corresponds to the first peak in Fig. 11. However, the particle cannot be captured at the droplet front and reaches the rear of the droplet under the fluid flow effect given the distance between the particle and the droplet

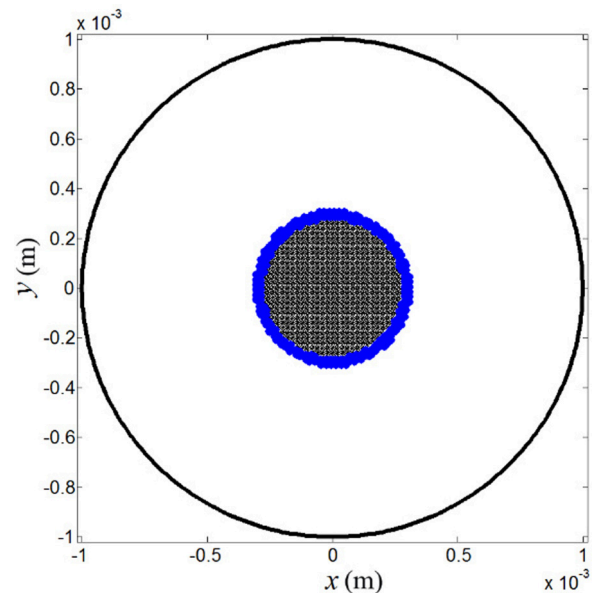


FIG. 10. (Color online) The distribution of the initial positions of captured particles with thermophoresis at  $Re = 150$  (white circle: the initial positions of the particles captured before flow separation; blue circle: the initial positions of the particles captured after flow separation).

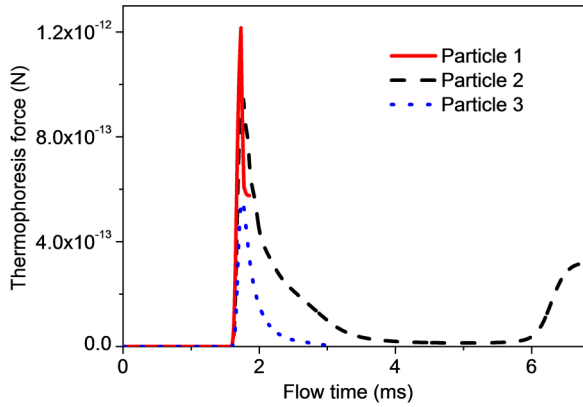


FIG. 11. (Color online) The change of the thermophoresis forces exerted on the particles moving in three motion patterns over time at  $Re = 150$ .

at this time. The difference of this situation from the one in which the thermophoretic force does not exist lies in the fact that the particle enters the closed vortex ring due to the thermophoretic force. The thermophoretic force is reduced to almost zero upon leaving the vicinity of the droplet and entering the vortex ring because the temperature gradient in the wake is small [Fig. 5(c)]. Then, the fluid carries the particle back to the vicinity of the droplet surface. The thermophoretic force increases again to correspond to the second peak in Fig. 11. Eventually, the particle is captured at the rear of the droplet. The effect of the thermophoretic force on the motion of Particle 3 is consistently weak. Moreover, the distribution of the temperature gradient shows that the high temperature gradient is limited to the vicinity of the droplet surface. Particle 3 is farther away from the droplet surface in subsequent motion because its initial position is farther from the center axis than the other two particles are. Thus, the thermophoretic force is weak and the particle cannot be captured.

Generally, two mechanisms contribute to the capture of particles under the thermophoresis effect. First, the particles move to the region at which thermophoresis is strong and deviates from the streamlines due to this force; the particle is captured directly. This scenario is illustrated in the figure depicting temperature distribution [Fig. 5(c)]. The effective region of thermophoresis remains within the vicinity of the droplet surface alone. Another mechanism is that the thermophoresis will exert a velocity directing to the inner of the vortex on the particle that was not captured before the separation point. The particle enters the closed vortex ring. The particle that has left the droplet moves to the vicinity of the droplet again under a circulatory flow in the vortex and is deposited on the rear of the droplet. In this process, the flow pattern and thermophoresis jointly influence the behavior of particle motion.

## V. BEHAVIOR OF PARTICLE MOTION AND DEPOSITION IN STEADY PLANE-SYMMETRIC FLOW

Section III A states that the flow is planar symmetric at  $Re = 250$ . Only the particles injected from the symmetric plane ( $x, z$ ) exhibit two-dimensional movement, as per Fig. 12(a). The movements of the other particles are three dimensional,

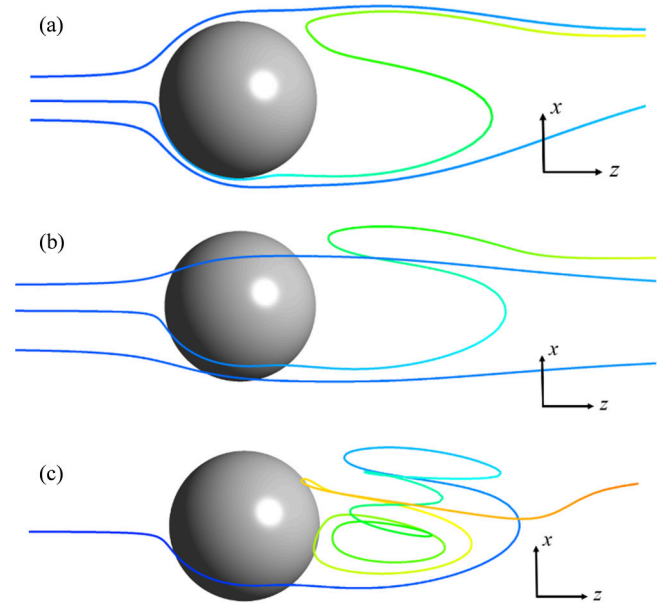


FIG. 12. (Color online) Trajectories of particles without thermophoresis at  $Re = 250$ .

as shown in Figs. 12(b) and 12(c). Without thermophoresis, the particle cannot be captured by the droplet. Most of the particles bypass the droplet directly and flow downstream. However, this flow differs from the flow when  $Re < 210$ . The vortex ring is no longer closed in the planar symmetric flow condition. The particle that started from the position near the centerline in the lower part penetrates the gap between vortices *a* and *b* and then flows downstream, as depicted in Fig. 12(b). Otherwise, the particle can flow directly into vortex *a*. Then, the particle follows the fluid flow inside the vortex and enters vortex *b* before eventually flowing out of the vortex, as indicated in Fig. 12(c).

With thermophoresis, the particles injected from the symmetric plane ( $x, z$ ) move two dimensionally, as depicted in Fig. 13(a). Some of the particles located near the centerline are captured at the droplet front; a few particles flow into vortex *b* and follow the fluid to the vicinity of the droplet to be captured. If the initial position is far from centerline, then the particles bypass the droplet and cannot be captured. The movement of particles injected from the other plane is three dimensional. The captured particles exhibit three motion patterns. The particle injected from the vicinity of the central line (Particle 1) is captured by the droplet surface at the droplet front, as shown in Fig. 13(b). Particles bypass the droplet front through only two deposition paths: one is by entering vortex *b* directly and then flowing back to the vicinity of the droplet following the fluid to be captured, as demonstrated by Particle 2 in Fig. 13(b). The other is by entering vortex *a* from the lower part, following the fluid, and then being captured at the rear, as indicated by Particle 3 in Fig. 13(c). The particle is ultimately deposited on the droplet surface by vortex *b* regardless of which vortex the particle enters initially. The particle from the upper part cannot enter directly into vortex *a* because of the flow in the upper part of the vortex. Figure 5(b) suggests that the streamline at the front of vortex *a* opposes the particle flow direction, which prevents particles from entering vortex *a* from

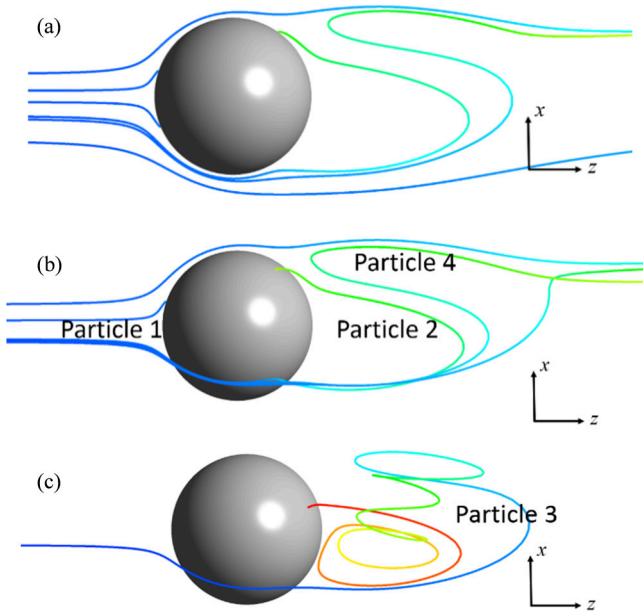


FIG. 13. (Color online) Trajectories of particles with thermophoresis at  $Re = 250$ .

the upper part. Although the flow pattern at this time varies from an axisymmetric flow, the mechanism by which flow pattern and thermophoresis jointly influence the behavior of particle motion is the same as that described when  $Re = 150$ .

Under steady flow condition, the initial position of particles determine their subsequent motion behavior. The distribution of initial position of captured particles corresponds well with the above three kinds of motion patterns. Figure 14 shows the initial position of particles that can be captured from a group of particles injected uniformly from plane  $(x, y)$ .

The flow is symmetric at plane  $(x, z)$ ; therefore, the distribution region of the initial position of the captured particles is symmetric at the projection of this plane on plane  $(x, y)$  (namely, axis  $x$ ). This process differs from that in an axisymmetric flow. In addition, the initial region of captured particles is divided into two parts. In the ring that has a certain interval with the main capture region (a continuous region consisting of black and blue dots from which most of the injected particles are captured), another part of the particles (denoted by red dots) can be captured. This finding contradicts the common knowledge that the particles near to the center axis line are easily captured. Different colors are used to distinguish the three motion behaviors of captured particles as described previously. The black dots denote particles that are captured before the separation point if they originate from this region. The particles initially injected from the blue region flow into vortex  $b$  directly and deposit after the flow separation point. The red particles in the ring region outside the gap correspond to the motion of Particle 3 in Fig. 13(c). The particles flow into vortex  $a$  first, then flow past vortex  $b$  and are captured eventually. The reason for such a gap between these two capture regions is that this portion of the particles enters the region between vortices  $a$  and  $b$ ; the particles flow toward the upper part of the vortex ring and then flow away following the fluids, as per the trajectory of Particle 4 in Fig. 13(b).

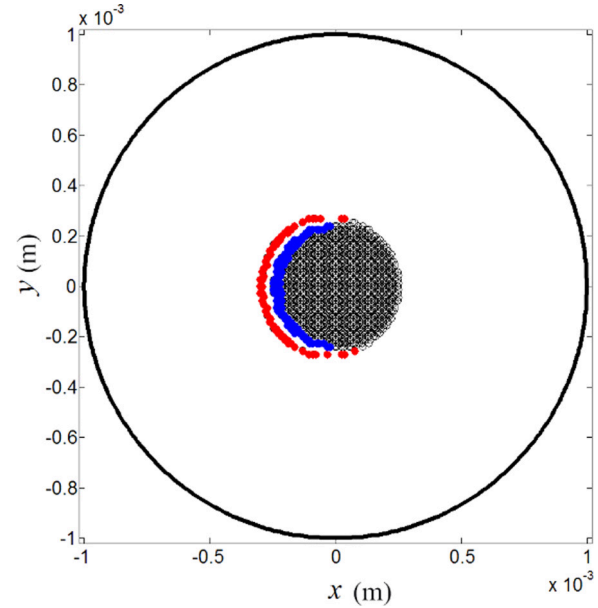


FIG. 14. (Color online) The distribution of the initial positions of captured particles with thermophoresis at  $Re = 250$  [white and blue (dark gray) denote the initial position of particles that deposit on the droplet by means of Particle 1 and Particle 2; red (light gray) (left separated dots) denotes the initial position of particles that deposit on the droplet by means of Particle 3].

## VI. BEHAVIOR OF PARTICLE MOTION AND DEPOSITION IN UNSTEADY PLANE-SYMMETRIC FLOW

When  $Re = 300$ , the flow enters the unsteady plane-symmetric state and the wake sheds periodically. The motion and deposition behaviors of the particles flowing around the front part of the droplet are similar to those in the previously described  $Re$  because the wake changes do not affect the flow at the droplet front. Therefore, we mainly discuss the particle behavior of motion and deposition at the rear of the droplet in the following section. We release the particles from the inlet plane and cause the time at which they flow by the separation point to correspond precisely to the four typical moments presented in Fig. 7(a). Particle motion is similar when the particles flow into the wake at the growing stage of the vortex (they flow past separation point at  $t = 0$  and  $t = 1/4\tau$ ). The external fluid can enter vortex  $a$  directly from the upper part this time because vortex  $a$  is constantly growing. Therefore, the particles can flow into vortex  $a$  even without thermophoresis, as shown in Fig. 15(a). However, particles still escape from the wake after flowing by vortex  $b$ . Although the flow is in the unsteady state, the distribution of flow field and temperature field all resemble those at  $Re = 250$  topologically. Therefore, the motion behaviors of other particles are similar to those at  $Re = 250$ . With thermophoresis, the particles flowing into vortex  $a$  directly from the upper part are pushed back to the vicinity of the droplet by the fluids and are captured under the effect of thermophoretic force, as depicted in Fig. 15(b). Despite the unsteady flow, the motion behaviors of the captured particles starting from the lower part are similar to those at  $Re = 250$ . The particles can enter vortices  $a$  and  $b$  directly from the lower part. Nonetheless, the particles deposit on the

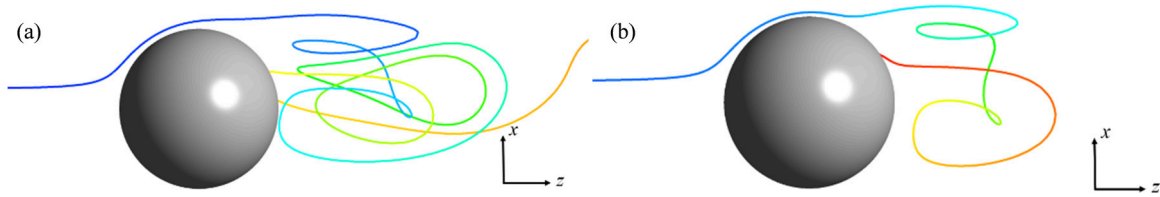


FIG. 15. (Color online) Trajectories of particles injected from the upper part at the growing stage of the vortex (at  $t = 0$  and  $t = 1/4\tau$ ) (a) without thermophoresis, and (b) with thermophoresis.

droplet surface by vortex  $b$  regardless of which vortex the particles enter. The difference between the two vortices is that movement is diversified in terms of motion behavior. As shown in Fig. 16(b), particles flow between vortices  $a$  and  $b$ , thus increasing their residence time in the wake to approximately 90 ms, which is roughly 13 times the vortex shedding period. Vortex shedding occurs 13 times when the particle flows in the vortex. Several periodical velocity fluctuations occur in the region through which particles flow. Under the unsteady flow condition, the particles that enter the wake are not necessarily captured by the droplet as a result of the periodical fluctuation in the region through which the particles flow. Nonetheless, the particles certainly cannot flow back to the rear of the droplet under fluid carriage and must not be captured if they cannot enter the wake. This claim can be proven by the distribution of the initial positions of the captured particles.

The particles that start from the upper part cannot enter vortex  $a$  directly when the particles flow into the wake at the vortex shedding stage (they flow past the separation point at  $t = 2/4\tau$  and  $t = 3/4\tau$ ) because at this point, the wake moves to the rear and sheds. Thus, the particles cannot enter vortex  $a$  but follow the fluids and flow away. The motion behavior of particles injected from the lower part are similar to that of the particles entering the wake at the vortex growing stage ( $t = 0$  and  $t = 1/4\tau$ ), as indicated in Fig. 16. The particles can either enter vortex  $b$  from the lower part or enter vortex  $a$  and flow through vortex  $b$  for capture by the droplet.

Two groups of uniformly distributed particles are injected from the inlet (Fig. 2) at different times. When one group of particles reaches the vicinity of the separation point, the vortex is at the growing stage. When the other group of particles reaches the vicinity of the separation point, the vortex is at the shedding stage. The initial position distribution of captured particles is shown in Fig. 17 and corresponds precisely with the motion behavior of particles; when particles enter the wake at the vortex growing stage, many particles can be captured outside the main capture region in the positive  $x$  axis, as per Fig. 17(a). This portion of the particles (blue dots) corresponds to the particles that enter vortex  $a$ . Many particles can be

captured outside the main capture region as well in the negative  $x$  axis; these particles are denoted by red dots. The motion behavior at  $Re = 250$  is described in detail; that is, the particles enter vortex  $a$  first and then flow through vortex  $b$  before capture. These initial positions of the captured particles are not continuous but disperse greatly. The blue and red dots indicate the dispersion state rather than the continuous main capture region and signify that the particles captured after the separation point must enter the wake, whereas the particles that enter the wake are not definitely captured. This outcome is attributed to the fact that the capture of particles depends on whether they can be transported to the vicinity of the droplet surface after they enter the wake. Assuming that one particle is captured by the droplet, another particle whose initial position is near the aforementioned particle may not be transported to the droplet surface by fluids because the second particle experiences the effect of several unsteady flows caused by the periodical vortex shedding, although this particle has entered the wake.

The flow field corresponding to the situation shown in Fig. 17(b) prevents the particles from entering vortex  $a$  from the upper part. Therefore, the particles injected from the positive  $x$  axis can only deposit before the separation point. No blue dot is observed in this figure.

As per the aforementioned motion behaviors throughout the entire vortex shedding period, the unsteady flow causes the initial positions of captured particles to change with time under the effect of thermophoresis. The capture probability of the particles injected from their initial positions during the vortex shedding period is depicted in Fig. 18. The probability of the particles being injected from the main capture region (red region) is 100%. Outside the main capture region, a large number of the particles that can be captured are scattered. Unsteady flow expands the scope of particle capture. The probability of capture is less than 1 beyond this region, thus indicating that the particle injected from this position can be captured at a certain time. As the flow at the rear of the droplet changes with time, the particle injected from this position may not be captured at another time.

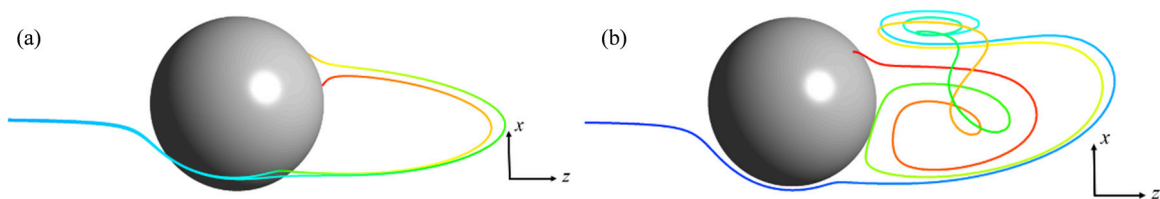


FIG. 16. (Color online) Trajectories of particles injected from the lower part at the growing stage of the vortex (at  $t = 0$  and  $t = 1/4\tau$ ) with thermophoresis.

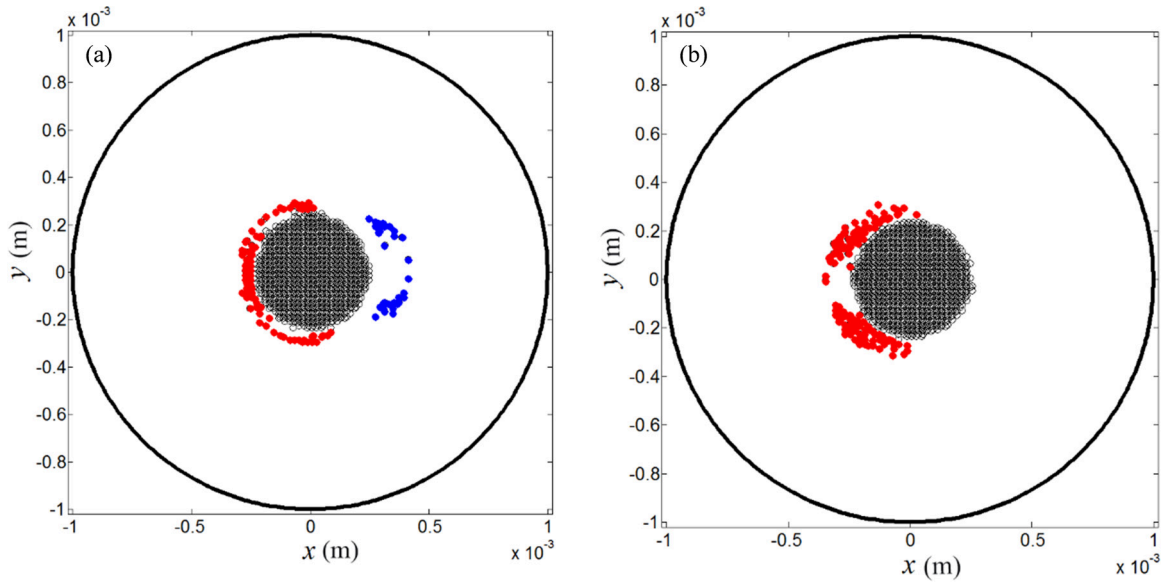


FIG. 17. (Color online) The distribution of the initial positions of captured particles with thermophoresis at  $Re = 300$  [white: the initial positions of the particles captured before flow separation; blue (dark gray) (right separated dots): the initial positions of the particles that enter vortex  $a$  from the upper part; red (light gray) (left separated dots): the initial positions of the particles that flow into vortex  $a$  first, then flow past vortex  $b$  and are captured eventually]. (a) Particles injected at the growing stage; (b) particles injected at the shedding stage.

Over ten vortex shedding periods, 60 groups of particles were uniformly injected from the inlet. The deposition distribution of the particles at the rear of the droplet is recorded. In Fig. 19, the outermost black circle represents the projection of the droplet on the plane  $(x, y)$ . The black dots are particles that deposit on the rear surface of the droplet. This figure shows that the deposition distribution is symmetric at axis  $x$  because axis  $x$  is positioned precisely at the projection of a symmetric plane [plane  $(x, z)$ ] on plane  $(x, y)$ . Particles deposit more on the positive axis  $x$  part and less on both the negative axis  $x$  part and the vicinity of axis  $x$ . This deposition distribution characteristic is closely related to the dynamic behavior of

particles. On the basis of the discussion above, particles deposit mainly on the droplet through vortex  $b$ . As per Fig. 16(a), a portion of the particles is transported to positive axis  $x$  through vortex  $b$ , and another portion is transported to negative axis  $x$ . This latter portion is near the surface of the droplet. Therefore, the particles deposit with strong thermophoretic force and are captured immediately. Only a few particles can be further transported to negative axis  $x$ ; therefore, few particles are deposited on negative axis  $x$ . Few particles can deposit on the vicinity of the projection axis of the symmetric plane because no velocity vector penetrates the symmetric plane.

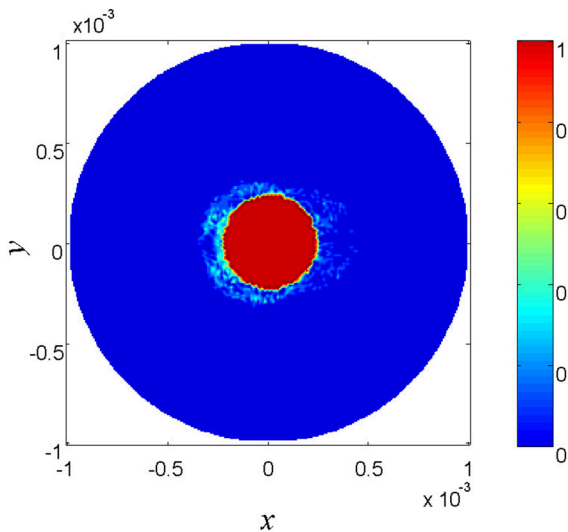


FIG. 18. (Color online) The capture probability of the particles injected from their initial positions during the vortex shedding period at  $Re = 300$ .

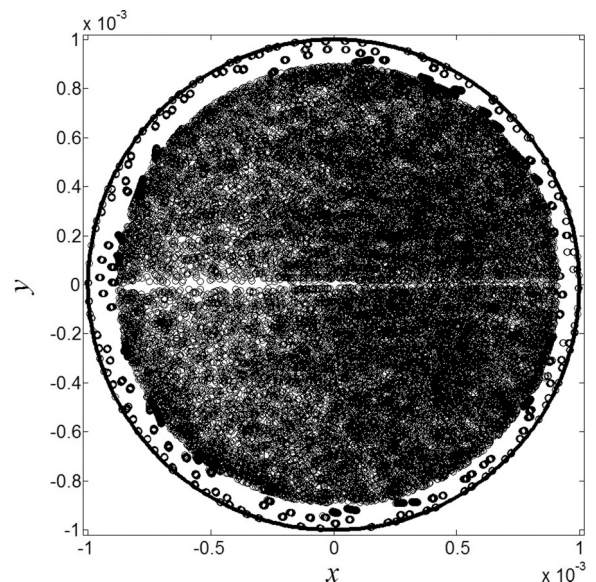


FIG. 19. The deposition distribution of the particles at the rear of the droplet at  $Re = 300$ .

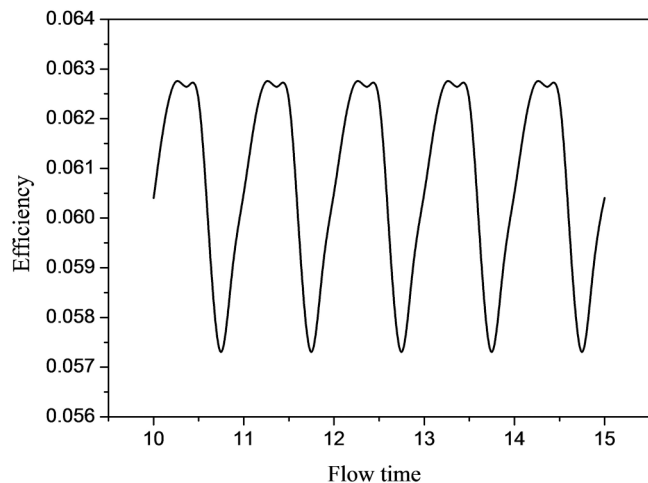


FIG. 20. Varying of the transient capture efficiencies with dimensionless flow time.

The difference caused by periodical vortex shedding varies the motion behavior of particles. Furthermore, the capture efficiencies are no longer constant at different times but change periodically over time. Figure 20 shows that the capture efficiencies shift periodically with dimensionless flow time. Dimensionless flow time is determined by dividing the actual time by the vortex shedding period. The period of efficiency oscillation is similar to that of the vortex shedding period. The relative oscillation amplitude of capture efficiency reaches 12.1% at  $Re = 300$ , and the lowest point of efficiency corresponds to the time when the vortex sheds completely.

## VII. CONCLUSION

The present study conducted three-dimensional direct numerical simulation to quantify the characteristics of the flow and temperature fields around a droplet at three typical  $Re$  values ( $Re = 150, 250, 300$ ) in the event of boundary-layer separation. The thermophoretic motion behavior of submicron particles was studied in these cases.

The flow is steady and axisymmetric at  $Re = 150$ . The thermophoretic motion of submicron particles can be divided into three patterns: the particle injected from the vicinity of the central axis line is captured by the droplet surface before the flow separation point; the particle injected from the position that is a certain distance from the central axis enters the closed vortex ring, flows in the vortex region, and is eventually captured on the back of the droplet; and the particle that is injected further from the central axis bypasses the droplet and cannot be captured. The initial injection region of the captured particles is circular because of the axisymmetric distribution of flow and temperature. The particles that are injected near

the center are easy to capture. Meanwhile, the deposition distribution of particles on the droplet surface is also circular.

The flow is steady planar symmetric at  $Re = 250$ , but the thermophoretic motion patterns of submicron particles change. The movements of the other particles are three dimensional, with the exception of those injected from the symmetric plane. Under the thermophoresis effect, some of the particles that start near the centerline are captured at the droplet front. A few particles flow into vortices *a* or *b* but eventually follow the fluid to the vicinity of the droplet through vortex *b* for capture. The distribution region of initial position of the captured particles is symmetric rather than asymmetric and circular. A portion of the particles that are injected outside the main capture region can be captured because the wake is no longer a closed vortex ring.

The flow behind the droplet enters the unsteady planar symmetric state at  $Re = 300$ . The unsteady flow influences only the particle behaviors of motion and deposition at the rear of the droplet. The periodical growth and shedding of the vortex cause the initial positions from which particles can enter the wake to change with time. At the vortex growing stage, particles may enter vortex *a* from the upper part, which is impossible at the vortex shedding stage. The motion behaviors of captured particles starting from the lower part are similar to those of the particles at  $Re = 250$ . After the flow separation point, only particles that have entered the wake can be captured. The residence time of particles after entering the wake is considerably longer than the vortex shedding period. The region through which the particles flow experiences several periods of velocity fluctuations, which generates the flow of particles between two vortices. The region from which the captured particles are injected undergo an obvious periodical change with vortex shedding. A large number of particles that can be captured are scattered outside the main capture region. This region changes periodically with time. The periodical change in wake causes the oscillation amplitude of capture efficiency to reach 12.1%.

The flow field and temperature field distribution characteristics of the three types of boundary-layer-separation flows are different, which lead to different thermophoretic motion and deposition patterns of submicron particles. The drag force of fluid and thermophoresis force contribute jointly to the deposition of submicron particles after boundary-layer separation around a droplet.

## ACKNOWLEDGMENTS

This work was supported by the fund from the National Natural Science Foundation of China (Grant No. 51576109) and the National Basic Research Program of China (973 Program) (Grant No. 2013CB228506).

- [1] Q. Zhang, K. He, and H. Huo, *Nature* **484**, 161 (2012).  
 [2] F. Dominici, M. Greemstone, and C. R. Sunstein, *Science* **344**, 257 (2014).

- [3] K. S. Lim, S. H. Lee, and H. S. Park, *J. Aerosol Sci.* **37**, 1826 (2006).  
 [4] S. Y. Bae, C. H. Jung, and Y. P. Kim, *J. Aerosol Sci.* **41**, 266 (2010).

- [5] A. Jaworek, W. Balachandran, A. Krupa, J. Kulon, and M. Lackowski, *Environ. Sci. Technol.* **40**, 6197 (2006).
- [6] N. E. L. Haugen and S. Kragset, *J. Fluid Mech.* **661**, 239 (2010).
- [7] E. G. Alexis, G. Marco, N. I. Gregory, and L. J. Nicole, *J. Fluid Mech.* **733**, 171 (2013).
- [8] D. M. Chate, P. Murugavel, K. Ali, S. Tiwari, and G. Beig, *Atmos. Res.* **99**, 528 (2011).
- [9] S. Y. Bae, C. H. Jung, and Y. P. Kim, *J. Aerosol Sci.* **40**, 621 (2009).
- [10] M. J. Pilat and A. Prem, *Atmos. Environ.* **10**, 13 (1976).
- [11] Z. G. Li and H. Wang, *Phys. Rev. E* **70**, 021205 (2004).
- [12] K. DeBleecker, A. Bogaerts, and W. Goedheer, *Phys. Rev. E* **71**, 066405 (2005).
- [13] R. Paredes V., V. Idler, A. Hasmy, V. Castells, and R. Botet, *Phys. Rev. E* **62**, 6608 (2000).
- [14] A. Guha, *Annu. Rev. Fluid Mech.* **40**, 311 (2008).
- [15] C. J. Tsai, J. S. Lin, S. G. Aggarwal, and D. R. Chen, *Aerosol Sci. Tech.* **38**, 131 (2004).
- [16] H. J. Keh and P. Y. Chen, *AIChE J.* **49**, 2283 (2003).
- [17] L. Schouweiler and M. Provansal, *Phys. Fluids* **14**, 3846 (2002).
- [18] H. M. Davenport and L. K. Peters, *Atmos. Environ.* **12**, 997 (1978).
- [19] P. K. Wang, S. N. Grover, and H. R. Pruppacher, *J. Atmos. Sci.* **35**, 1735 (1978).
- [20] S. Viswanathan, *Ind. Eng. Chem. Res.* **38**, 4433 (1999).
- [21] G. Dau, *Chem. Eng. Technol.* **10**, 330 (1987).
- [22] A. Querel, M. Monier, A. I. Flossmann, P. Lemaitre, and E. Porcheron, *Atmos. Res.* **142**, 57 (2014).
- [23] R. Hassanzadeh, B. Sahin, and M. Ozgoren, *Int. J. Comput. Fluid. Dyn.* **25**, 535 (2011).
- [24] K. Gumowski, J. Miedzik, S. Goujon-Durand, P. Jenffer, and J. E. Wesfreid, *Phys. Rev. E* **77**, 055308 (2008).
- [25] T. A. Johnson and V. C. Patel, *J. Fluid Mech.* **378**, 19 (1999).
- [26] S. Lee, *Comput. Fluids* **29**, 639 (2000).
- [27] A. G. Tomboulides and S. A. Orszag, *J. Fluid Mech.* **416**, 45 (2000).
- [28] L. Talbot, R. K. Cheng, R. W. Schefer, and D. R. Willis, *J. Fluid Mech.* **101**, 737 (1980).
- [29] A. Richter and P. A. Nikrityuk, *Int. J. Heat Mass Transfer* **55**, 1343 (2012).